Supporting Information for

Structure property relationships affecting the proton conductivity in imidazole loaded Al-MOFs

Thomas Homburg[1], Caroline Hartwig[1], Helge Reinsch[1], Michael Wark[2], Norbert Stock[1]

1. Preparation of imidazole-loaded frameworks
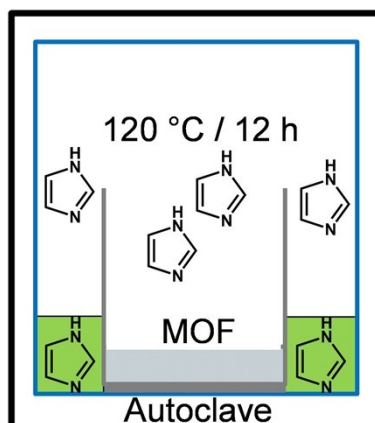
Figure S1: The MOFs (~ 30 mg) were placed in a 2 mL Teflon insert (gray). Another 30 mL Teflon insert (blue) was filled with 500 mg imidazole (HIm). The smaller insert was placed into the larger Teflon sleeve and placed in a steel autoclave (black) at 120 °C for 12 h, with 1 h heating up and 1 h cooling down to yield **1_HIm**, **2_HIm**, and **3_HIm**, respectively. **4_HIm** was obtained within 4 h at 120 °C.

2. Thermogravimetric analyses

The amount of imidazole molecules in **1_**, **2_**, **3_** and **4_HIm** was evaluated by thermogravimetric analysis (TGA).
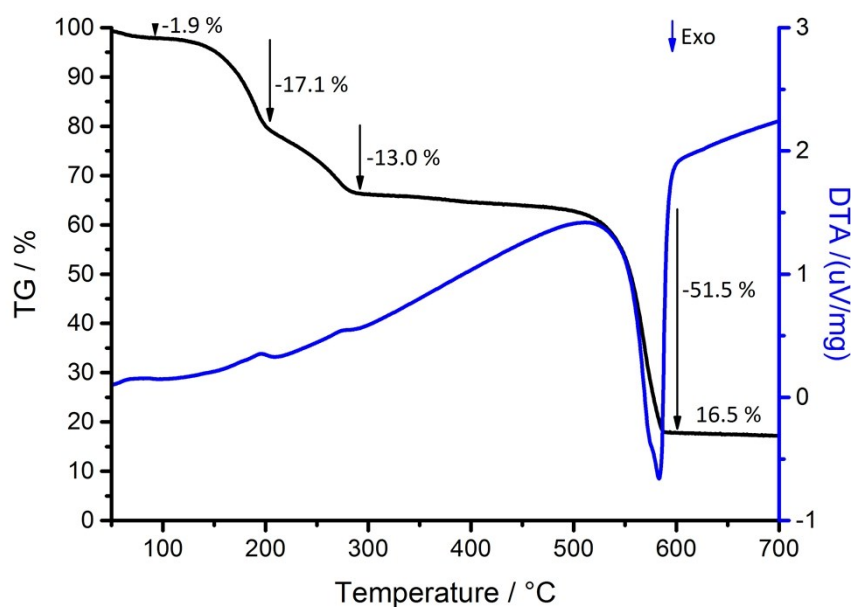
Figure S2: TG curve of MIL-53_HIm, [Al(OH)(BDC)]·1.3HIm, measured in air.
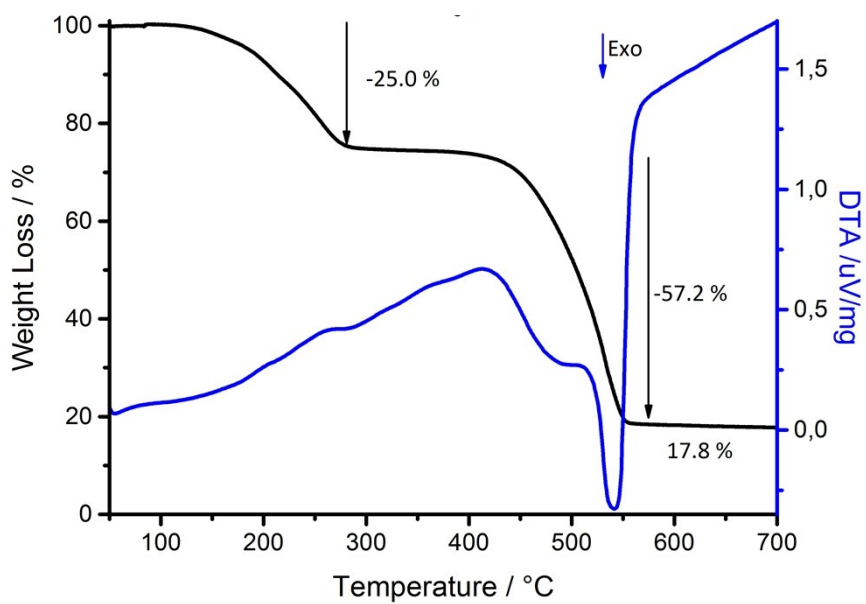
Figure S3: TG curve of MIL-53-CH$_3$_HIm, [Al(OH)(BDC-(CH$_3$))]·1.2HIm, measured in air.
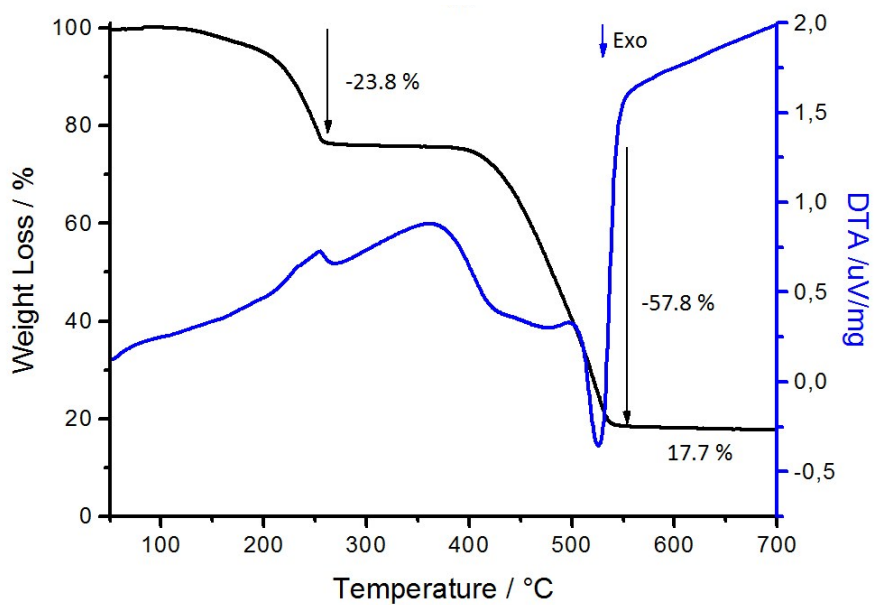
Figure S4: TG curve of MIL-53-(CH$_3$)$_2$_HIm, [Al(OH)(BDC-(CH$_3$)$_2$)]·1.1HIm, measured in air.
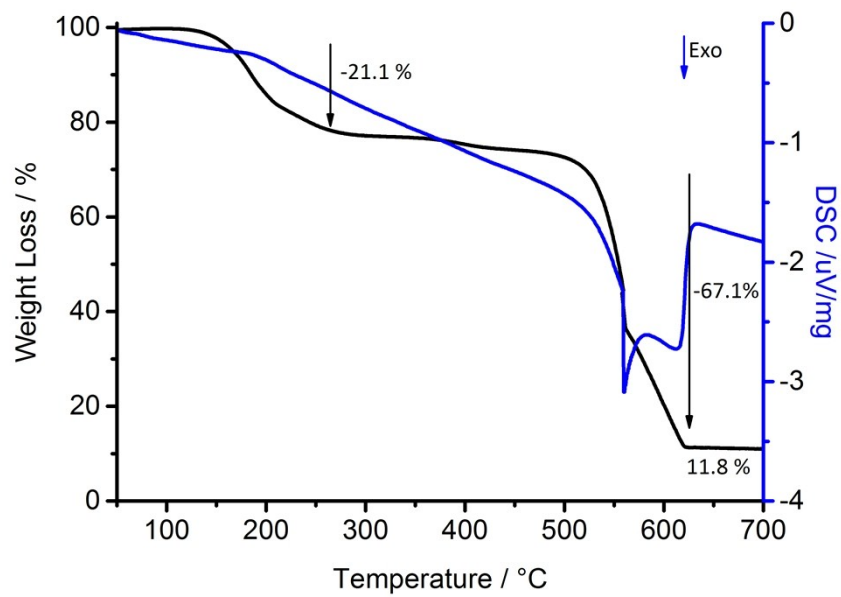
Figure S5: TG curve of CAU-11_HIm, [Al(OH)(SDBS)]·1.3HIm, measured in air.

3. ^{1}H-NMR spectroscopy

The amount of imidazole molecules in **1_**, **2_**, **3_** and **4_HIm** was evaluated by dissolving the host-guest compounds in 5wt% NaOD/D$_2$O and measuring ^{1}H-NMR spectra. Integration of the signals yields the molar ratios of imidazole : linker molecules.
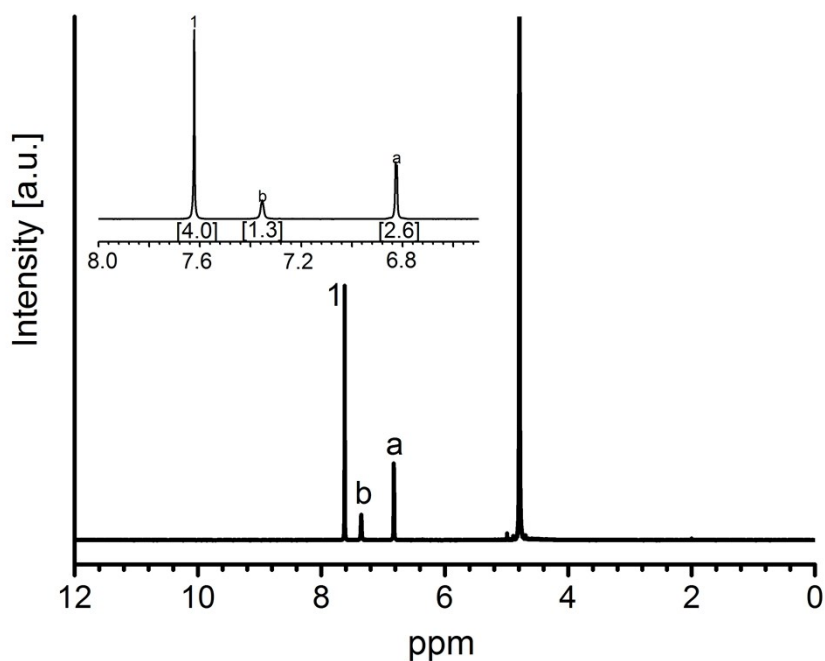
Figure S 6: ^{1}H-NMR spectrum of dissolved MIL-53_HIm.
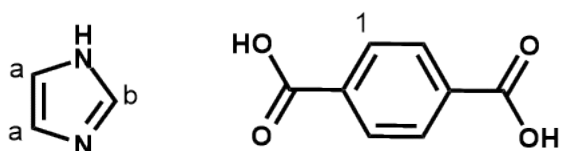
^{1}**H-NMR:** (500 MHz, D$_2$O, 300K): δ=7.62 (s, 4H, H-1), 7.35 (s, 1.3H, H-b), 6.82 (s, 2.6H, H-a) ppm.
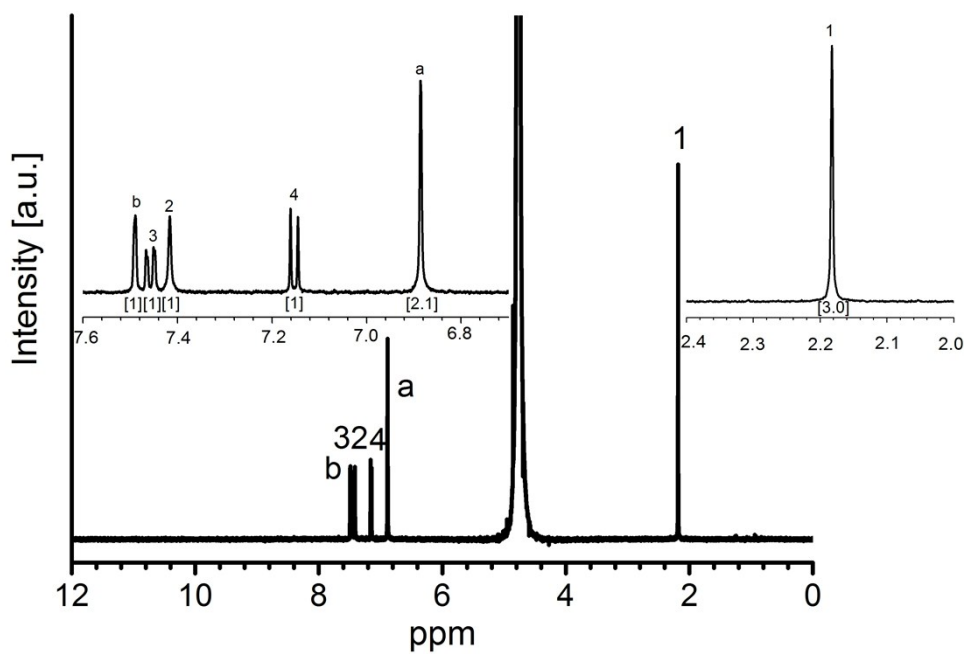
Figure S7: ^{1}H-NMR spectrum of dissolved MIL-53-CH$_3$_HIm.
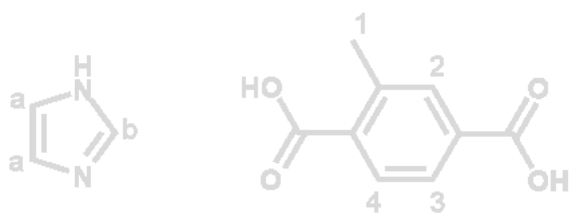
^{1}H-NMR: (500 MHz, D$_2$O, 300K): δ=7.49 (s, 1.2H, H-b), 7.46 (d, 1H, H-3, ^3J=8 MHz), 7.41 (s, 1H, H-2), 7.15 (d, 1H, H-4,^3J=8 MHz), 6.89 (s, 2.4H, H-a), 2.18 (s, 3H, H-1) ppm.
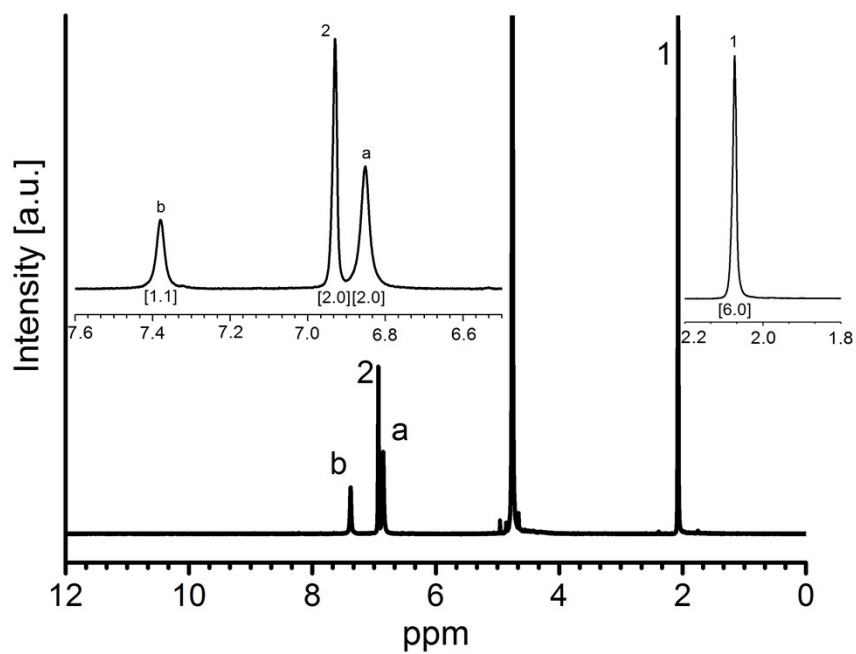
Figure S8: ^{1}H-NMR spectrum of dissolved MIL-53-(CH$_3$)$_2$_HIm.
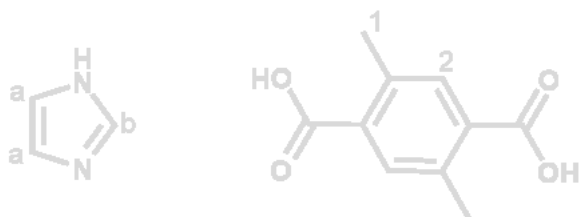
^{1}H-NMR: (500 MHz, D$_2$O, 300K): δ=7.37 (s, 1.1H, H-b), 6.92 (s, 2H, H-2), 6.84 (s, 2.2H, H-a), 2.07 (s, 6H, H-1) ppm.
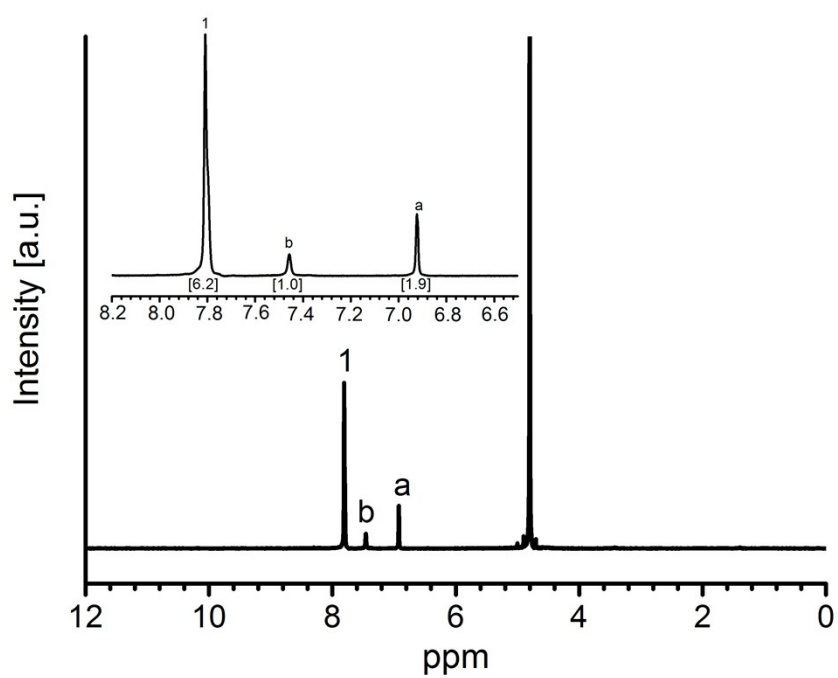
Figure S9: ^{1}H-NMR spectrum of dissolved CAU-11_HIm.
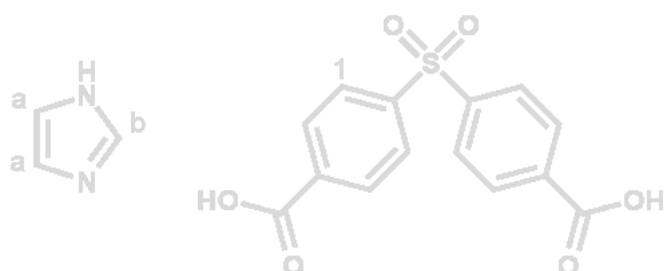
^{1}H-NMR: (500 MHz, D$_2$O, 300K): δ=7.81 (s, 6.2H, H-1), 7.42 (s, 1H, H-b), 6.94 (s, 1.9H, H-a) ppm.

4. Impedance spectroscopy

Measurements were carried out at 80, 90, 100, and 110 °C. In the following figures, only the data obtained at 110 °C is presented.

A Bode phase plot of the impedance was used to determine the Ohmic resistance. In a Bode plot, the impedance corresponding to the phase shift (red curve) closest to zero is approximately equal to the Ohmic resistance (black curve) of the sample.
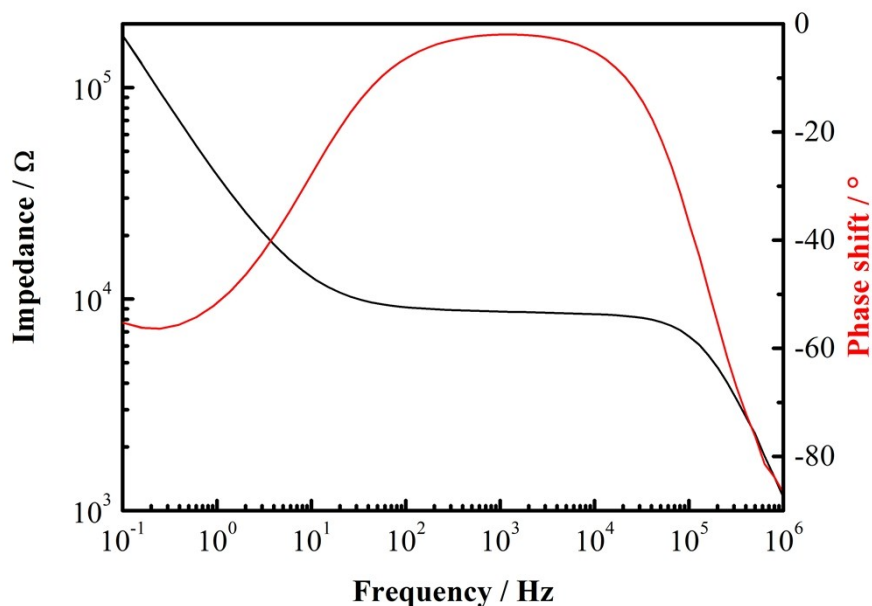
Figure S10: Bode-plot of powder impedance data of MIL-53_HIm at 110 °C.
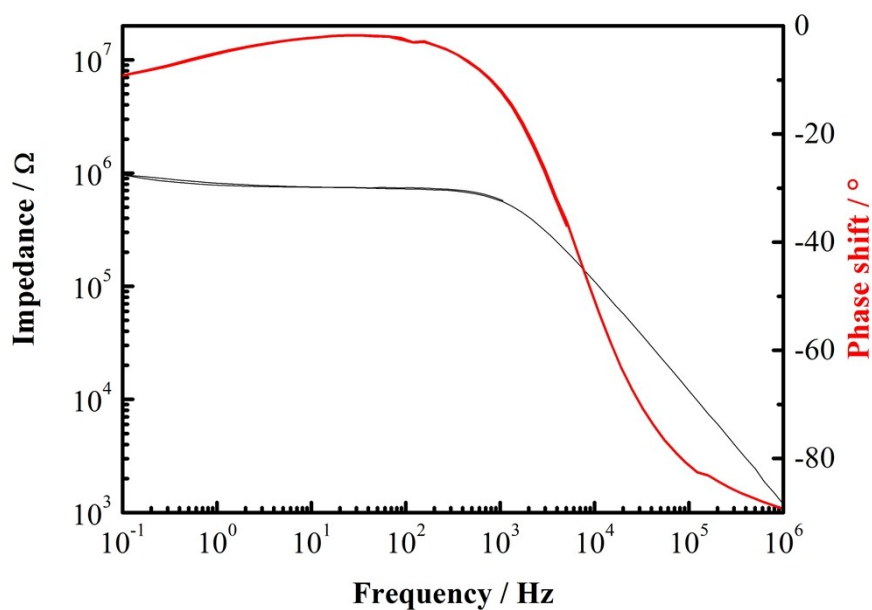
Figure S11: Bode-plot of powder impedance data of MIL-53-CH_3_HIm at 110 °C.
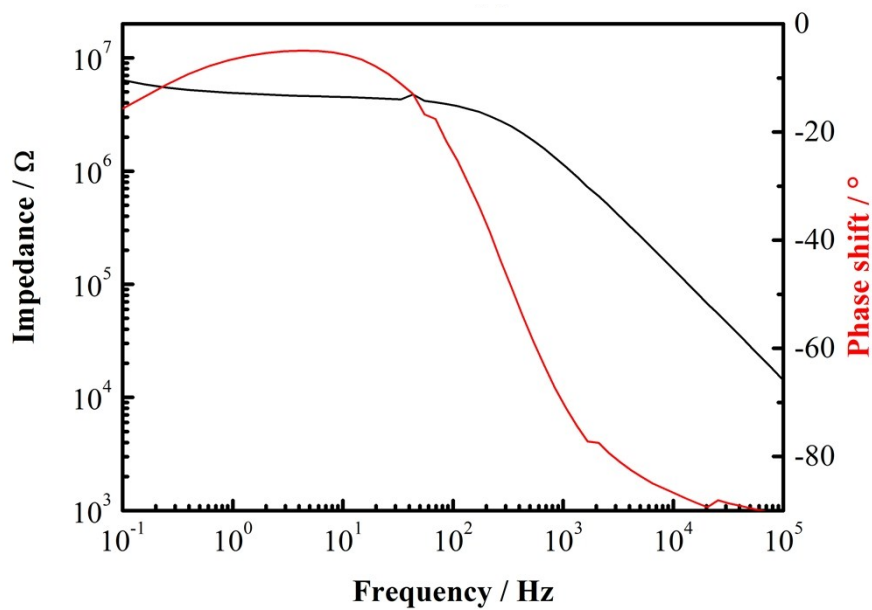
FIgure S12: Bode-plot of powder impedance data of MIL-53-$(CH_3)_2$_HIm at 110 °C.
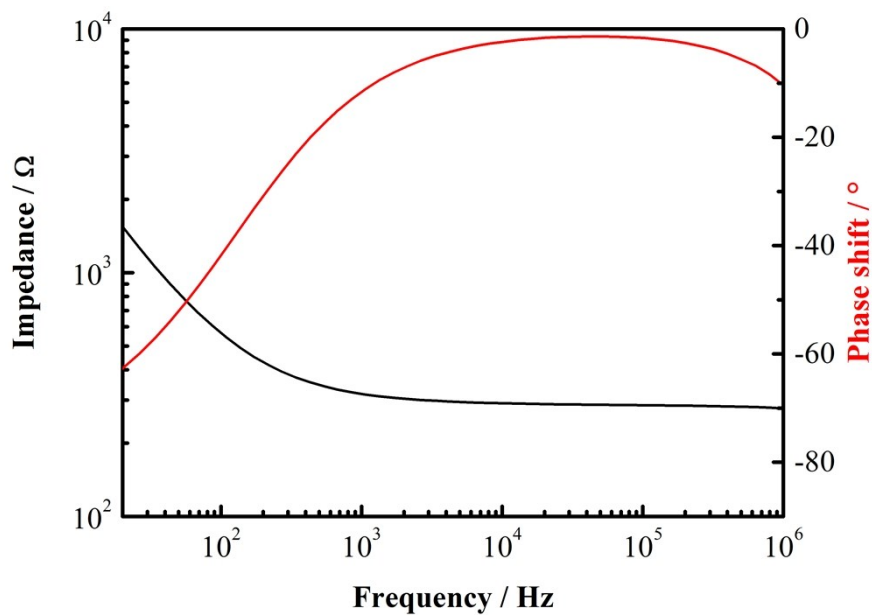
Figure S13: Bode-plot of powder impedance data of CAU-11_HIm at 110 °C.

5. IR-spectroscopy

The anti-symmetric (1590-1550 cm^{-1}) and symmetric (1390-1370 cm^{-1}) C-O stretching vibrations of the carboxylate groups are present in the spectra of all eight compounds. The methyl-functionalized compounds show very weak C-H stretching modes (2985-2920 cm^{-1}) and a band associated with the deformation vibration of the methyl group (1395 cm^{-1}). The signal at ~2850 cm^{-1} is characteristic for hydrogen bonded imidazole oligomers and is marked with an asterisk (*).[1]
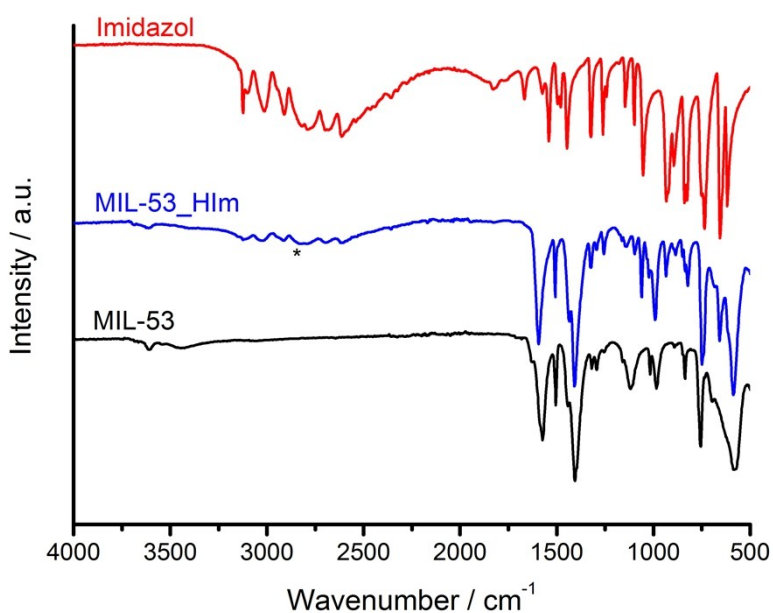
Figure S14: IR-spectra of MIL-53 (black), MIL-53_HIm (blue) and imidazole (red). In MIL-53 and MIL-53_HIm, the signals around 3600 cm^{-1} are in both cases clearly observable. In addition, a signal at 2850 cm^{-1} is observed (marked with *), which is characteristic for hydrogen bonded imidazole oligomers.
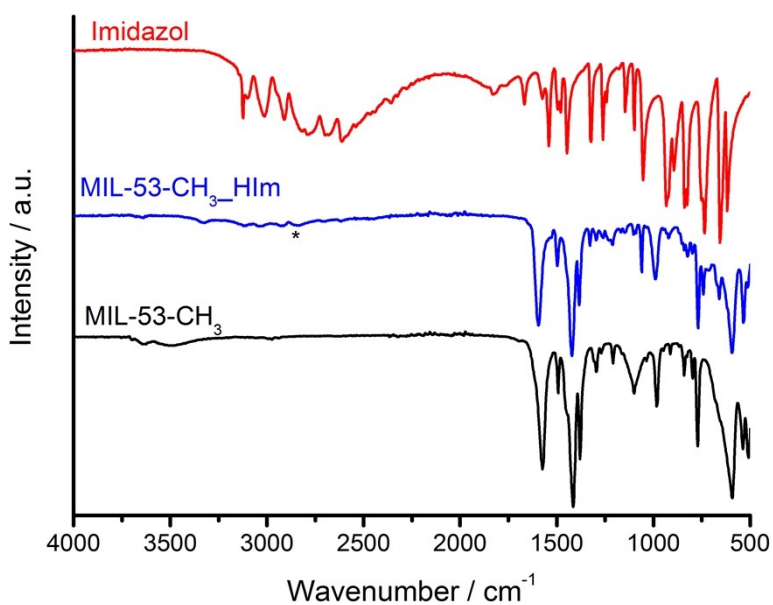
Figure S15: IR-spectra of MIL-53-CH$_3$ (black), MIL-53-CH$_3$_HIm (blue) and imidazole (red). If one compares MIL-53-CH$_3$ to MIL-53-CH$_3$_HIm, a decrease of the signal intensity around 3600 cm^{-1} is observed. However, comparing pure imidazole and MIL-53-CH$_3$_HIm only a weak signal at 2850 cm^{-1} (marked with a *) for the host-guest compound is noticeable.
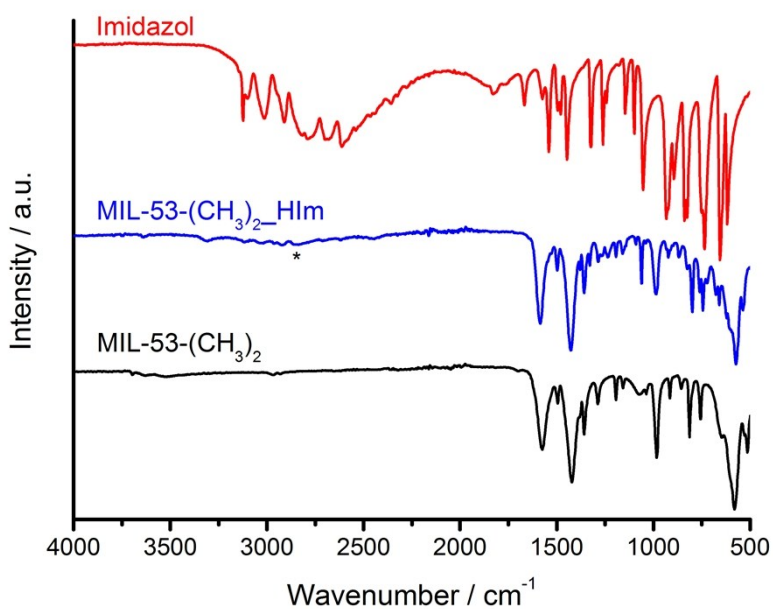
Figure S16: IR-spectra of MIL-53-(CH$_3$)$_2$ (black), MIL-53-(CH$_3$)$_2$_HIm (blue) and imidazole (red). If one compares MIL-53-(CH$_3$)$_2$ and MIL-53-(CH$_3$)$_2$_HIm, a decrease of the signal intensity around 3600 cm^{-1} is observed. However, comparing pure imidazole and MIL-53-(CH$_3$)$_2$_HIm only a weak signal at 2850 cm^{-1} (marked with a *) are noticeable in MIL-53-(CH$_3$)$_2$_HIm.
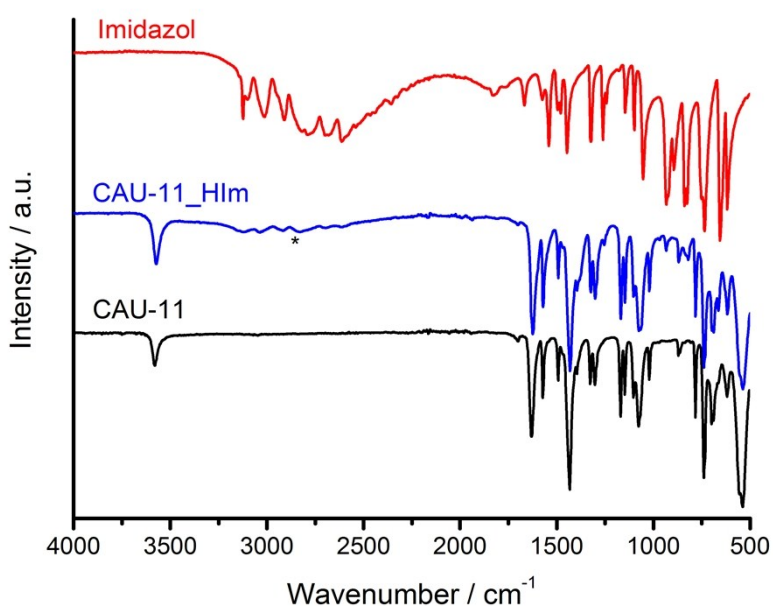
Figure S17: IR-spectra of CAU-11 (black), CAU-11_HIm (blue) and imidazole (red). In CAU-11 and CAU-11_HIm a strong signal at 3580 cm^{-1} is observed. In addition, a distinct band at 2850 cm^{-1} is found (marked with an asterisk, *) for CAU-11_HIm.

6. Crystal structure determinations

The crystal structures of the imidazole loaded MOFs were determined by Rietveld refinement of PXRD data. The reader should therefore take into account that the distinction between nitrogen and carbon atoms in the imidazole rings is rather tentative since the difference in electron density of these elements is too small to reliably distinguish these two species.

In order to set up a starting model for Al-MIL-53_HIm, the pattern was indexed, suggesting a primitive orthorhombic unit cell which is similar to the unit cell of Al-MIL-53-*as*.[2] Al-MIL-53-*as*, which contains disordered linker molecules in the channels, was therefore used as a starting model for force-field optimizations. The universal force field as implemented in Materials Studio, was used after setting the cell parameters to the indexed values and removing the original guest molecules. Subsequently, imidazole molecules were generated and structurally optimized using the same program. The molecules were placed inside the channels using Materials Studio and this structural model was employed for further Rietveld

13

refinement with TOPAS academics. The two observed imidazole molecules were refined as rigid bodies with varying occupancies. The framework atoms were freely refined, except for the lateral atoms of the benzene rings which had to be fixed at their position. The refinement converged to sufficient figures of merit with two independent imidazole molecules. However, the observed loading in Rietveld refinement is slightly higher (1.3 molecules per Al^{3+} ion), than in the TG experiment (1 imidazole per Al^{3+}ion).
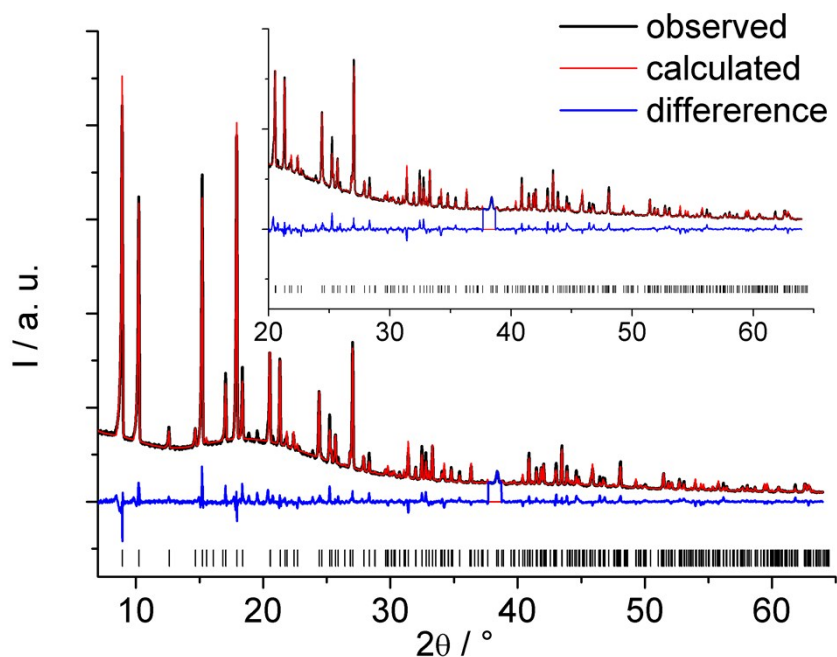
Figure S18: Rietveld plot for the refinement of Al-MIL-53-HIm. Black line gives the experimental data, red line gives the calculated curve, and the blue line the difference. Vertical bars mark the allowed Bragg positions. The section around 38 ° was excluded due to a peak of the sample holder.

The PXRD pattern of Al-MIL-53-CH_3_HIm was successfully indexed in a *C*-entered monoclinic unit cell, which is similar to the unit cell of Al-MIL-53-*lt*.[2] Al-MIL-53-*lt*, which contains water molecules in the channels, was thus used as a starting model for the force-field optimization, using Materials Studio after setting the cell parameters to the indexed values and adding the methyl group. Subsequently, one imidazole molecule was generated and structurally optimized using the same program. The molecule was placed inside the channel using Materials Studio and this structural model was used for further Rietveld refinement with TOPAS academics. The imidazole molecule and the carbon backbone of the linker molecule were refined as rigid bodies, also refining the occupancy of imidazole. All other framework atoms were freely refined. The Rietveld refinement converged to sufficient figures of merit

14

and the determined loading (1.00 molecule per Al^{3+} ion) compares well to the one obtained from the TG experiment (1 imidazole per Al^{3+} ion). Based on the distances between different imidazole rings, there could also be interactions between adjacent guest molecules, and not only between OH-groups of the host framework and the nitrogen atoms of the imidazole ring. However, the refinement using PXRD data is not sufficient to reliably distinguish between nitrogen and carbon atoms.
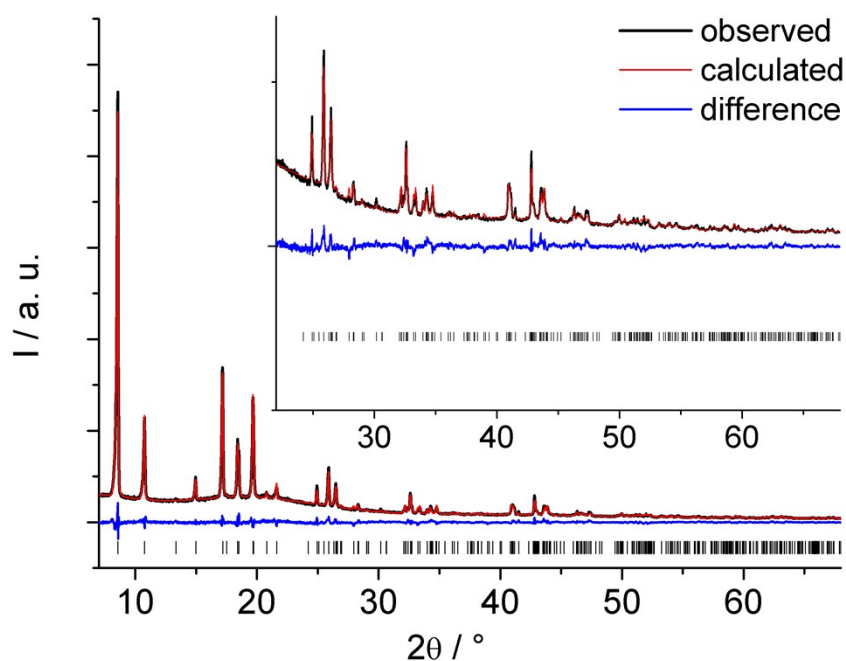
Figure S19: Rietveld plot for the refinement of Al-MIL-53-CH_3-HIm. Black line gives the experimental data, red line gives the calculated curve, and the blue line the difference. Vertical bars mark the allowed Bragg positions. The section around 38 ° was excluded due to a peak of the sample holder.

The PXRD pattern of Al-MIL-53-$(CH_3)_2$_HIm was successfully indexed, suggesting a primitive monoclinic unit cell with space group $P2_1/c$. Due to the indexed unit cell dimensions and the angle of this cell being close to 90°, we anticipated a similarity with the primitive orthorhombic unit cell of Al-MIL-53_HIm. Thus the orthorhombic unit cell of Al-MIL-53_HIm was converted into a monoclinic cell using a subgroup-supergroup relationship with the program Powdercell (sequence $Pnma \rightarrow P112_1/a = P2_1/c$).[3] This monoclinic model was used as a starting model for force-field optimization, using the universal force field implemented in Materials Studio after setting the cell parameters to the indexed values and adding the functional methyl groups. Subsequently, one imidazole molecule was generated and structurally optimized using the same program. The molecule was placed inside the channel

using Materials Studio and this structural model was used for further Rietveld refinement with TOPAS academics. The imidazole molecule and the carbon backbone of the linker molecule were both refined as rigid bodies, also refining the occupancy of imidazole. All other framework atoms were freely refined. The observed loading in Rietveld refinement is comparable (1.00 molecule per Al^{3+} ion) to the TG experiment (1 imidazole per Al^{3+} ion).
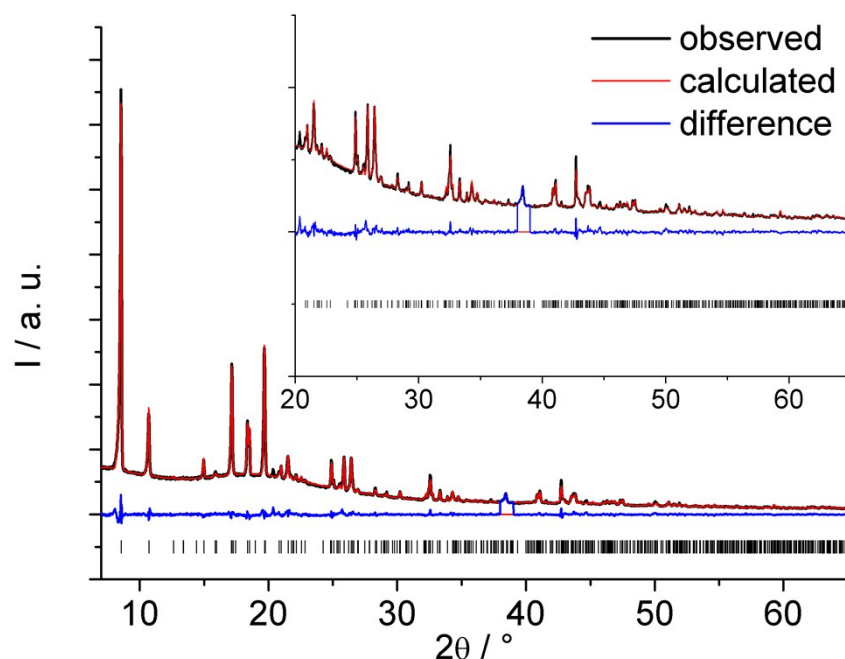
Figure S20: Rietveld plot for the refinement of Al-MIL-53-$(CH_3)_2$-HIm. Black line gives the experimental data, red line gives the calculated curve, and the blue line the difference. Vertical bars mark the allowed Bragg positions. The section around 38 ° was excluded due to a peak of the sample holder.

The PXRD pattern of CAU-11_HIm was successfully indexed suggesting a primitive orthorhombic unit cell with cell dimensions and symmetry comparable to those determined for the host compound CAU-11. The crystal structure of CAU-11 was therefore used as a starting model for force-field optimization, using the universal force field implemented in Materials Studio after setting the cell parameters to the indexed values. Subsequently, one imidazole molecule was generated and structurally optimized using the same program. The molecule was placed inside the MOF's channel using Materials Studio and this structural model was used for further Rietveld refinement with TOPAS academics. The imidazole molecule was refined as a rigid body, and the occupancy was also refined. All other framework atoms were freely refined. In order to match all observed reflections, crystalline imidazole was refined as a minor phase with a mass fraction of ≈ 8(4)%. The observed loading

16

in Rietveld refinement is comparable (0.74 molecules per Al^{3+} ion) to the TG experiment (0.8 imidazole per Al^{3+} ion). However, while the rigid body guest molecules in the MIL-53 structures arrange in positions that allow the deduction of reasonably strong interactions with OH-groups or aromatic moieties, the guest molecules in CAU-11 are found in the center of the channels, indicating only very weak interactions with the host framework. Moreover, the guest molecules are located too close to each other to give a chemically sensible arrangement. Thus, the refined structure of CAU-11_HIm should be rather interpreted as randomly confined guest molecules in a crystalline framework.
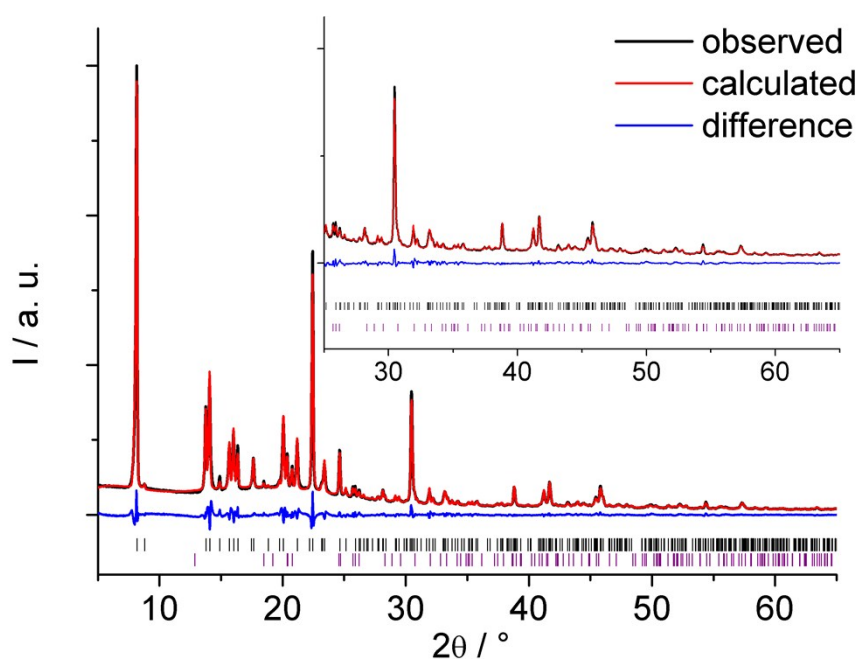
Figure S21: Rietveld plot for the refinement of CAU-11-HIm. Black line gives the experimental data, red line gives the calculated curve, and the blue line the difference. Vertical bars mark the allowed peak positions for CAU-11-HIm, while purple bars mark the peak positions for imidazole.

Table S1: Summary of the crystallographic parameters of the Rietveld refinements of MIL-53_imi, MIL-53-CH$_3$_imi, MIL-53-(CH$_3$)$_2$_imi and CAU-11_imi.

	MIL-53_HIm	MIL-53-CH$_3$_HIm	MIL-53-(CH$_3$)$_2$_HIm	CAU-11_HIm
formula sum	C$_{11}$H$_{11}$O$_5$N$_2$Al	C$_{12}$H$_{13}$O$_5$N$_2$Al	C$_{13}$H$_{15}$O$_5$N$_2$Al	C$_{14}$H$_{15}$O$_7$N$_2$S$_1$Al
wavelength	CuKα_1	CuKα_1	CuKα_1	CuKα_1
a [Å]	17.2406(4)	17.6626(7)	6.6052(2)	6.6149(3)
b [Å]	6.6342(2)	13.2531(5)	13.2296(5)	12.8493(5)
c [Å]	12.0503(2)	6.6111(3)	16.4981(5)	20.0971(6)
β [°]	90	111.585(3)	89.472(2)	90
volume /Å^3	1378.28(5)	1439(2)	1441.6(1)	1708.2(1)
space group	*Pnma*	*Cc*	*P2$_1$/c*	*Pnma*
R$_{WP}$ / %	4.8	4.9	3.6	5.4
R$_{Bragg}$ / %	4.3	1.6	1.5	1.2
GoF	2.98	2.61	2.12	1.92

```
data_
_chemical_name_mineral Al-MIL-53_HIm
_cell_length_a  17.24056(38)
_cell_length_b  6.63418(15)
_cell_length_c  12.05029(24)
_cell_angle_alpha 90
_cell_angle_beta  90
_cell_angle_gamma 90
_cell_volume 1378.276(51)
_symmetry_space_group_name_H-M PNMA
loop_
_symmetry_equiv_pos_as_xyz
    '-x, -y, -z'
    '-x, y+1/2, -z'
    '-x+1/2, -y, z+1/2'
    '-x+1/2, y+1/2, z+1/2'
    'x, -y+1/2, z'
    'x, y, z'
    'x+1/2, -y+1/2, -z+1/2'
    'x+1/2, y, -z+1/2'
loop_
_atom_site_label
_atom_site_type_symbol
_atom_site_fract_x
_atom_site_fract_y
_atom_site_fract_z
_atom_site_occupancy
_atom_site_B_iso_or_equiv
Al10 Al 0 0 0 1 0.50(17)
O1 O 0.00477(93) -0.25 -0.07626(67) 1 0.50(17)
C1 C 0.09173(49) -0.25 0.13375(68) 1 0.50(17)
C2 C 0.11554(67) 0.25 -0.1214(10) 1 0.50(17)
O2 O 0.07348(35) -0.0723(11) 0.11753(40) 1 0.50(17)
O3 O 0.08461(41) 0.0874(12) -0.09289(58) 1 0.50(17)
C3 C 0.20284 -0.06752 0.23385 1 0.50(17)
C4 C 0.22724 0.0678 -0.2087 1 0.50(17)
C5 C 0.16726 -0.25 0.20206 1 0.50(17)
C6 C 0.19107 0.25 -0.18119 1 0.50(17)
C10b C 0.345269 -0.167447 0.005316017 0.3755(32) 0.50(17)
N11b N 0.3920416 -0.2850262 0.07201559 0.3755(32) 0.50(17)
C12b C 0.4507302 -0.1644795 0.1129526 0.3755(32) 0.50(17)
C13b C 0.4402195 0.02760296 0.07155078 0.3755(32) 0.50(17)
N14b N 0.375046 0.02577358 0.005034245 0.3755(32) 0.50(17)
C10 C 0.3863983 0.142242 0.05348799 0.2845(32) 0.50(17)
N11 N 0.410855 -0.03268242 0.1047281 0.2845(32) 0.50(17)
C12 C 0.4690954 0.01711468 0.1783936 0.2845(32) 0.50(17)
N13 N 0.4806246 0.2228247 0.1726767 0.2845(32) 0.50(17)
C14 C 0.4295191 0.3001551 0.09548887 0.2845(32) 0.50(17)
```

```
data_
_chemical_name_mineral Al-MIL-53-CH3_HIm
_cell_length_a  17.66262(66)
_cell_length_b  13.25314(51)
_cell_length_c  6.61113(31)
_cell_angle_alpha 90
_cell_angle_beta  111.5853(33)
_cell_angle_gamma 90
_cell_volume 1439.04(11)
_symmetry_space_group_name_H-M CC
loop_
_symmetry_equiv_pos_as_xyz
     'x, -y, z+1/2'
     'x, y, z'
     'x+1/2, -y+1/2, z+1/2'
     'x+1/2, y+1/2, z'
loop_
_atom_site_label
_atom_site_type_symbol
_atom_site_fract_x
_atom_site_fract_y
_atom_site_fract_z
_atom_site_occupancy
_atom_site_B_iso_or_equiv
Al1 Al -0.00573(78) 0.0000(10) 0.0378(19) 1 0.87(12)
O2 O -0.0109(14)  0.05832(93) 0.2836(24) 1 0.87(12)
O3 O 0.08470(55) -0.0849(11) 0.5562(16) 1 0.87(12)
O4 O 0.41928(93) -0.3948(15) 0.5482(28) 1 0.87(12)
O5 O 0.07463(88) -0.09948(95) 0.2023(22) 1 0.87(12)
O6 O 0.41739(96) -0.4095(13) 0.8649(17) 1 0.87(12)
C7 C 0.104696 -0.1119959 0.4054688 1 0.87(12)
C8 C 0.3866968 -0.3721744 0.6780604 1 0.87(12)
C9 C 0.1955641 -0.2377796 0.6563478 1 0.87(12)
C10 C 0.3006738 -0.2411429 0.4281324 1 0.87(12)
C11 C 0.2644692 -0.2996659 0.7267245 1 0.87(12)
C12 C 0.2337067 -0.1771553 0.357736 1 0.87(12)
C13 C 0.1786841 -0.176596 0.4708565 1 0.87(12)
C14 C 0.3165842 -0.3033664 0.611633 1 0.87(12)
C15 C 0.225607 -0.1078468 0.1708659 1 0.87(12)
C20 C -0.5743166 0.1375109 -0.2200492 1.0000(91) 0.87(12)
C16 C -0.5502936 0.05314906 -0.2926193 1.0000(91) 0.87(12)
N17 N -0.4970559 0.07962464 -0.3925781 1.0000(91) 0.87(12)
C18 C -0.4879105 0.1804837 -0.3822903 1.0000(91) 0.87(12)
N19 N -0.5354858 0.2134167 -0.2768283 1.0000(91) 0.87(12)
```

data_

_chemical_name_mineralAl-MIL-53-(CH3)2_HIm
_cell_length_a 6.60517(21)
_cell_length_b 13.22955(46)
_cell_length_c 16.49809(48)
_cell_angle_alpha 90
_cell_angle_beta 89.4717(24)
_cell_angle_gamma 90
_cell_volume 1441.599(80)
_symmetry_space_group_name_H-M P21/C
loop_
_symmetry_equiv_pos_as_xyz
    '-x, -y, -z'
    '-x, y+1/2, -z+1/2'
    'x, -y+1/2, z+1/2'
    'x, y, z'
loop_
_atom_site_label
_atom_site_type_symbol
_atom_site_fract_x
_atom_site_fract_y
_atom_site_fract_z
_atom_site_occupancy
_atom_site_B_iso_or_equiv
Al1 Al 0 0 0 1 1.02(13)
Al2 Al 0.5 0 0 1 1.02(13)
O1 O 0.2495(25) 0.06933(87) -0.0022(13) 1 1.02(13)
O2 O 0.0912(12) -0.4141(12) 0.41231(60) 1 1.02(13)
O3 O 0.4198(12) -0.4093(10) 0.41831(51) 1 1.02(13)
O4 O 0.0907(12) -0.10170(96) 0.07524(59) 1 1.02(13)
O5 O 0.4174(12) -0.09528(99) 0.08129(61) 1 1.02(13)
C6 C 0.25242 -0.12547 0.10846 1 1.02(13)
C7 C 0.25805 -0.39909 0.38118 1 1.02(13)
C8 C 0.24747 -0.19502 0.17844 1 1.02(13)
C9 C 0.26299 -0.32954 0.31119 1 1.02(13)
C10 C 0.10109 -0.26243 0.30266 1 1.02(13)
C11 C 0.42030 -0.32950 0.25191 1 1.02(13)
C12 C 0.09016 -0.19506 0.23772 1 1.02(13)
C13 C 0.40937 -0.26213 0.18698 1 1.02(13)
C14 C 0.59749 -0.40113 0.25353 1 1.02(13)
C15 C -0.08703 -0.12345 0.23610 1 1.02(13)
C16a C -0.3446312 -0.07074141 -0.5613716 1.0000(66) 1.02(13)
C17a C -0.4132599 -0.1692548 -0.5621427 1.0000(66) 1.02(13)
N18a N -0.2782303 -0.2276112 -0.5191621 1.0000(66) 1.02(13)
C19a C -0.1261566 -0.1651657 -0.4918328 1.0000(66) 1.02(13)
N20a N -0.1671936 -0.06820943 -0.517919 1.0000(66) 1.02(13)

data_
_chemical_name_mineral CAU-11_HIm
_cell_length_a 6.61491(26)
_cell_length_b 12.84934(47)
_cell_length_c 20.09706(59)
_cell_angle_alpha 90
_cell_angle_beta 90
_cell_angle_gamma 90
_cell_volume 1708.19(10)
_symmetry_space_group_name_H-M PNMA
loop_
_symmetry_equiv_pos_as_xyz
    '-x, -y, -z'
    '-x, y+1/2, -z'
    '-x+1/2, -y, z+1/2'
    '-x+1/2, y+1/2, z+1/2'
    'x, -y+1/2, z'
    'x, y, z'
    'x+1/2, -y+1/2, -z+1/2'
    'x+1/2, y, -z+1/2'
loop_
_atom_site_label
_atom_site_type_symbol
_atom_site_fract_x
_atom_site_fract_y
_atom_site_fract_z
_atom_site_occupancy
_atom_site_B_iso_or_equiv
Al1 Al 0.0782(10) 0.75 0.24811(43) 1 0.50(12)
O1 O -0.1780(16) 0.75 0.20714(62) 1 0.50(12)
O2 O 0.4983(11) 0.64506(64) 0.19018(42) 1 0.50(12)
O3 O 0.1633(11) 0.64267(64) 0.18579(45) 1 0.50(12)
C1 C 0.1632(13) 0.48825(62) 0.08905(48) 1 0.50(12)
C2 C 0.1733(13) 0.40256(65) 0.04718(51) 1 0.50(12)
C3 C 0.3557(12) 0.35543(60) 0.03561(51) 1 0.50(12)
C4 C 0.5361(12) 0.38843(64) 0.06293(54) 1 0.50(12)
C5 C 0.5215(11) 0.47199(59) 0.10554(43) 1 0.50(12)
C6 C 0.3407(13) 0.52117(59) 0.11965(42) 1 0.50(12)
C7 C 0.3334(15) 0.60895(66) 0.17078(48) 1 0.50(12)
S1 S 0.3814(16) 0.25 -0.01844(42) 1 0.50(12)
O4 O 0.2053(33) 0.25 -0.05928(93) 1 0.50(12)
O5 O 0.5987(29) 0.25 -0.04879(95) 1 0.50(12)
C10 C 0.1383963 0.3430715 0.2411933 0.3727(34) 0.50(12)
N11 N 0.1107114 0.2366656 0.2454196 0.3727(34) 0.50(12)
C12 C -0.0929692 0.2171692 0.2392993 0.3727(34) 0.50(12)
C13 C -0.1911723 0.3115343 0.2312919 0.3727(34) 0.50(12)
N14 N -0.04817612 0.3893373 0.2324614 0.3727(34) 0.50(12)

[1] H. Wolff, H. Müller, H. Müller, *Ber. Bunsenges. Phys. Chem.* **1974**, *78*, 1241-1244.

[2] T. Loiseau, C. Serre, C. Huguenard, G. Fink, F. Taulelle, M. Henry, T. Bataille, G. Férey, *Chem. Eur. J.* **2004**, *10*, 1373-1382.

[3] W. Kraus, G. Nolze, PowderCell 2.4, 2000.